PAPER

Polymeric architecture as a tool for controlling the reactivity of palladium(II) loaded nanoreactors†

Shreyas S. Wagle, [ID] [a,b] Parul Rathee, [ID] [a,b] Krishna Vippala, [ID] [a,b,c] Shahar Tevet, [ID] [a,b] Alexander Gordin, [ID] [d] Roman Dobrovetsky [ID] [a] and Roey J. Amir [ID] *[a,c,d,e]

Self-assembled systems, like polymeric micelles, have become great facilitators for conducting organic reactions in aqueous media due to their broad potential applications in green chemistry and biomedical applications. Massive strides have been taken to improve the reaction scope of such systems, enabling them to perform bioorthogonal reactions for prodrug therapy. Considering these significant advancements, we sought to study the relationships between the architecture of the amphiphiles and the reactivity of their Pd[II] loaded micellar nanoreactors in conducting depropargylation reactions. Towards this goal, we designed and synthesized a series of isomeric polyethylene glycol (PEG)-dendron amphiphiles with different dendritic architectures but with an identical degree of hydrophobicity and hydrophilic to lipophilic balance (HLB). We observed that the dendritic architecture, which serves as the main binding site for the Pd[II] ions, has greater influence on the reactivity than the hydrophobicity of the dendron. These trends remained constant for two different propargyl caged substrates, validating the obtained results. Density functional theory (DFT) calculations of simplified models of the dendritic blocks revealed the different binding modes of the various dendritic architectures to Pd[II] ions, which could explain the observed differences in the reactivity of the nanoreactors with different dendritic architectures. Our results demonstrate how tuning the internal architecture of the amphiphiles by changing the orientation of the chelating moieties can be used as a tool for controlling the reactivity of Pd[II] loaded nanoreactors.

1. Introduction

Despite the vital role of water as a solvent in nature in general and especially in living systems, it did not make its way into mainstream organic chemistry. Even today, most organic synthesis is carried out in dry organic solvents since many of the chemicals and reagents used are sparingly soluble in water. Amphiphilic polymers that self-assemble in water, where the hydrophobic portions collapse together because of the hydrophobic effect, can help bridge this gap between organic and aqueous phase chemistry.[1] Polymeric assemblies, including micelles and vesicles, have gained increasing attention due to their potential to serve as nanoreactors for conducting organic reactions in aqueous media.[2] These self-assembled structures have sizes in the nanometre range. They can host most hydrophobic substrates, effectively reducing the reaction volume and leading to a high local concentration of the substrate molecules. This phenomenon can eventually help in carrying out reactions in relatively milder conditions than conducting the corresponding reaction in an organic environment.[3–5] Additional advantages of utilizing these systems include the reduced consumption of volatile organic solvents and reduced chemical load on the environment.

Although the development of nanoreactors is in its emergent state, significant contributions have already been made, especially in facilitating organometallic and organocatalytic reactions using self-assembled polymeric amphiphiles as reported by Meijer,[6–8] Lipshutz,[5,9–11] Weck,[12–14] O'Reilly,[15–18] Zimmerman,[19–21] and many others.[22–26] Several studies have focused on understanding the effect of different ligands,[6–8,19,24,27] amphiphile's and substrate's hydrophobicity,[7,26] and the type of co-surfactants,[9,10] on the range and the type of the reactions that can be conducted in aqueous environment. In addition to these parameters, it is also important to further understand how the architecture of the amphiphiles and the resulting positioning and number of chelating moieties can affect the reactivity of the

[a]Department of Organic Chemistry, School of Chemistry, Faculty of Exact Sciences, Tel-Aviv University, Tel-Aviv 6997801, Israel. E-mail: amirroey@tauex.tau.ac.il
[b]Tel-Aviv University Center for Nanoscience and Nanotechnology, Tel-Aviv University, Tel-Aviv, 6997801, Israel
[c]Analytical Technologies Unit R&D, Teva Pharmaceutical Industries, Kfar Saba 4410202, Israel
[d]The ADAMA Center for Novel Delivery Systems in Crop Protection, Tel-Aviv University, Tel-Aviv, 6997801, Israel
[e]The Center for Physics and Chemistry of Living Systems, Tel-Aviv University, Tel-Aviv 6997801, Israel

self-assembled nanoreactors. Hence, we decided to systematically tune the position of the chelating moieties and the number of end-groups in the dendritic part of the amphiphile while maintaining their overall molecular weight and hydrophilic to lipophilic balance (HLB).[10] By using this approach, we aimed to isolate the effect of the dendritic architecture on reaction kinetics while minimizing the influence of other parameters. With this in mind, we synthesized a library of PEG-dendron amphiphiles with three, four, and six thioether containing end-groups in the dendritic part of the amphiphile (Fig. 1). The utilization of a dendritic structure as the lipophilic block allowed us to precisely tune the architecture and the lipophilicity of the dendritic block. This high molecular precision enabled us to synthesize amphiphiles with nearly identical molecular weights and HLB. In this study we used palladium-mediated O-propargyl cleavage[27–30] as a model reaction due to its potential application as bioorthogonal uncaging approach for the activation of dyes and prodrugs.[31–35] The suggested mechanisms of this palladium catalysed uncaging of propargylic substrates such as dyes and cytotoxic drugs has been recently reviewed by Domingos.[36]

To evaluate the impact of the type of protecting group on the reaction rate, we synthesized two low molecular weight substrates containing different propargyl protecting groups (propargyl ether and propargyl carbamate). These substrates were used as model prodrugs for conducting depropargylation reactions using Pd^{II}-loaded micellar nanoreactors with different dendritic architectures. This approach enabled us to investigate how the nano environment inside the micellar core, and the type of propargyl protecting group affect the reaction rates.

2. Results and discussion

Our amphiphiles were constructed from a commercial 5 kDa methoxy polyethylene glycol (mPEG$_{5k}$) as the hydrophilic block, and dendron as the lipophilic block. The dendritic architecture, and the number and length of the end-groups were varied to maintain the overall molecular weight and HLB of the amphiphiles to help us isolate the effect of their architecture on the kinetics.

2.1. Tuning the number of end-groups in dendron

Synthesis and characterization of amphiphiles. Three amphiphiles were synthesized: mPEG$_{5k}$-D-(C14)$_3$ (**C14×3**) (calculated M_n = 6081 Da), mPEG$_{5k}$-D-(C11)$_4$, (3,5) (**C11×4 (3,5)**) (calculated M_n = 6084 Da) and mPEG$_{5k}$-D-(C6)$_6$ (**C6×6**) (calculated M_n = 6094 Da). The **C14×3** amphiphile was synthesized by coupling mPEG$_{5k}$-NH$_2$ to an activated 4-nitrophenol ester of 3,4,5-tris(allyloxy)benzoic acid[37] to get mPEG$_{5k}$-triene followed by a thiol–ene reaction using 1-tetradecanethiol to obtain the amphiphile. For making the four-armed (3,5) amphiphile, **C11×4 (3,5)**, mPEG$_{5k}$-NH$_2$ was coupled with an activated 4-nitrophenol ester of 3,5-bis(prop-2-yn-1-yloxy) benzoic acid[37] to get mPEG$_{5k}$-di-yne (3,5), followed by thiol–yne reaction with 1-undecanethiol. To make the **C6×6** amphiphile, first the complete **C6×6** dendron was synthesized by propargylating gallic acid,[37] which was then coupled to 1-hexanethiol using thiol–yne chemistry. Finally, the **C6×6** dendron was conjugated to mPEG$_{5k}$-NH$_2$ to get the final amphiphile (Scheme 1). ^{1}H-NMR, High-Performance Liquid Chromatography (HPLC), and Gel Permeation Chromatography (GPC) were used to verify the conversion, product's purity, molecular weight and polydispersity, respectively. All experimental results showed excellent correlations with the expected values, as can be seen in the ESI.†

After synthesizing the amphiphiles, their self-assembly into micelles in aqueous media (phosphate buffered saline-PBS, pH 7.4, 37 °C) was examined by measuring their critical micelle concentration (CMC) values using the Nile red method.[38] The CMC values of all three amphiphiles were nearly identical (Table 1 and Fig. S20, S21 and S23†). Next, we used dynamic light scattering (DLS) to estimate the size of the micelles in the presence and absence of Pd^{II} salt. To prepare the metal loaded micelles, the Pd^{II} salt and the different amphiphiles were dissolved separately in acetone, mixed and stirred briefly, followed by the evaporation of acetone to form a thin film, which was rehydrated in PBS to yield aqueous micellar solutions ([amphiphile] = 320 μM). The diameters of the micelles measured by DLS were found to be around 20 nm (for the empty micelles), while slightly smaller diameters were
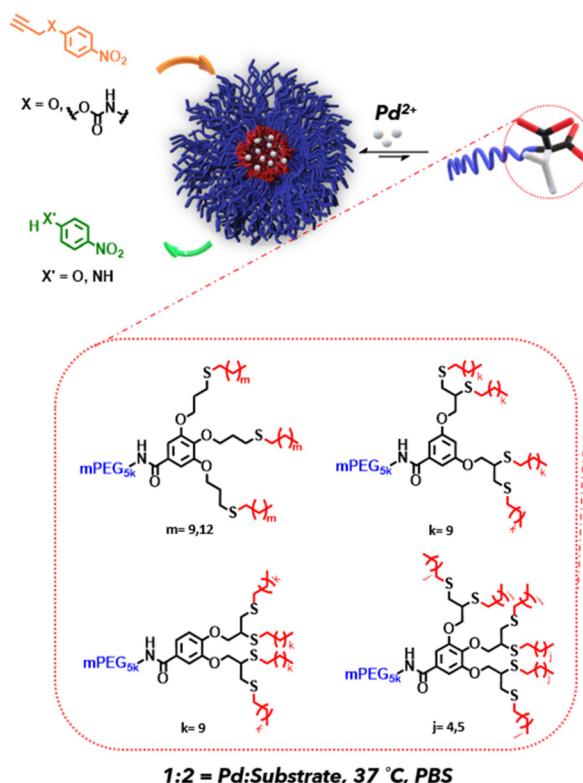

Fig. 1 Schematic illustration of Pd^{II}-loaded micellar nanoreactors based on PEG-dendron amphiphiles with varied architectures for the depropargylation of substrates with different propargyl protecting groups.
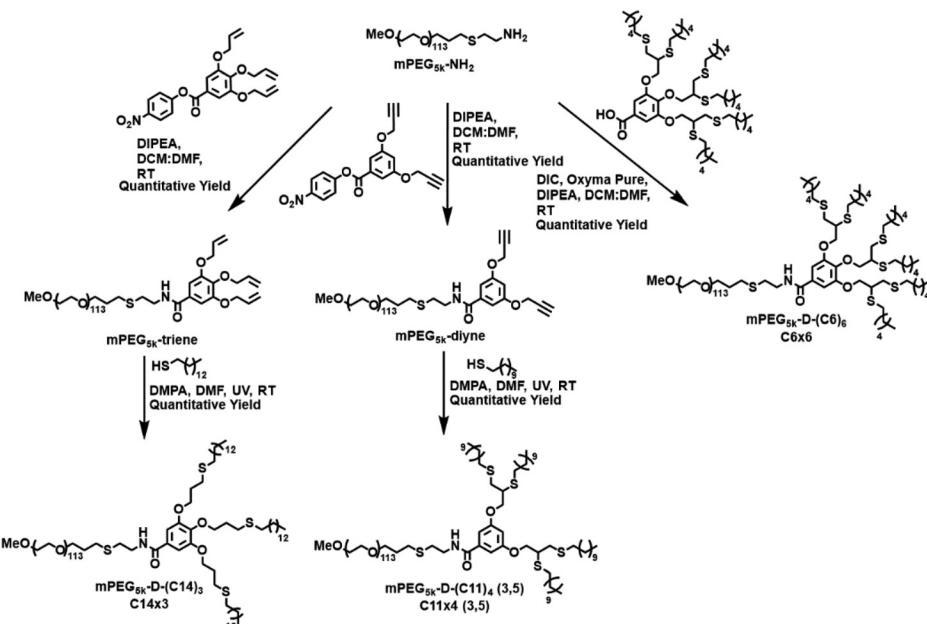
Scheme 1 Synthetic route for **C14×3**, **C11×4 (3,5)** and **C6×6** amphiphiles.

Table 1 Molecular properties of the **C14×3**, **C11×4 (3,5)** and **C6×6** amphiphiles and their micellar assemblies

Hybrid	Name	End-group	M_n^a (kDa)	M_n^b (kDa)	$Đ^b$	CMC^c (μM)	D_h^d (nm) [Pd] = 0 μM	D_h^e (nm) [Pd] = 75 μM	D_h^f (nm) [Pd] = 150 μM
mPEG$_{5k}$-D-(C14)$_3$	**C14×3**	n-C$_{14}$H$_{29}$	6.1	6.3	1.03	4 ± 1	24 ± 4	22 ± 2	20 ± 7
mPEG$_{5k}$-D-(C11)$_4$ (3,5)	**C11×4 (3,5)**	n-C$_{11}$H$_{23}$	6.1	6.3	1.04	4 ± 1	17 ± 1	15 ± 1	15 ± 2
mPEG$_{5k}$-D-(C6)$_6$	**C6×6**	n-C$_6$H$_{13}$	6.1	6.0	1.04	3 ± 1	20 ± 1	16 ± 1	16 ± 2

[a] Calculated based on a 5 kDa mPEG and the expected exact mass of the dendrons. [b] Measured by GPC using PEG commercial standards. [c] Determined using the Nile red method. [d] Hydrodynamic diameter measured by DLS (% volume) of micelles formed from micelles only ([amphiphile] = 320 μM). [e] Hydrodynamic diameter measured by DLS (% volume) of micelles ([amphiphile] = 320 μM) with the encapsulated Pd(OAc)$_2$ salt [75 μM]. [f] Hydrodynamic diameter measured by DLS (% volume) of micelles ([amphiphile] = 320 μM) with the encapsulated Pd(OAc)$_2$ salt [150 μM].
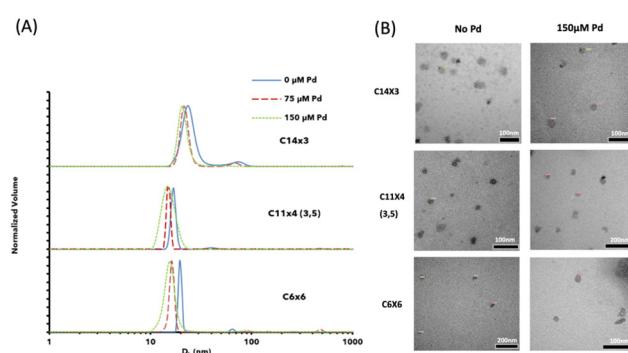

Fig. 2 (A) DLS measurements of micelles with different dendritic architectures ([amphiphile] = 320 μM) without encapsulated Pd(OAc)$_2$ (blue solid lines), micelles with encapsulated Pd^{II} ([Pd(OAc)$_2$] = 75 μM) (red large-dashed lines) and micelles with encapsulated Pd^{II} ([Pd(OAc)$_2$] = 150 μM) (green dashed lines) in PBS (pH = 7.4) at 37 °C. (B) TEM images of the micelles based on the **C14×3**, **C11×4 (3,5)** and **C6×6** amphiphiles, with (right column) and without (left column) Pd(OAc)$_2$ salt.

observed for Pd^{II}-loaded micelles (Table 1 and Fig. 2). Transmission electron microscopy (TEM) images of empty, and Pd^{II} loaded micelles further confirmed the presence of nano-sized spherical particles (Fig. 2 and Fig. S31†), which correlates with the data that was obtained from DLS.

The two substrates *para*-nitrophenyl propargyl ether (**PNPPE**)[26] and *N-para*-nitrophenyl *O*-propargyl carbamate (**PNACAPE**)[39] with propargyl ether and propargyl carbamate protecting groups, respectively, were synthesized as previously reported. The depropargylation reactions were conducted by adding the substrate, **PNPPE** (300 μM) and **PNACAPE** (150 μM) to micellar solutions containing 150 μM and 75 μM Pd^{II} respectively. The ratio of Pd^{II} to substrate was 1 : 2 in both cases. The reaction progress at 37 °C was monitored by HPLC (Fig. 3, and Fig. S34–S37, S40 and S41†).

To evaluate the rate of depropargylation, the area under the curve (AUC) of the substrate's peak in each chromatogram was measured (Fig. 3A) and the decrease in AUC (in %) was plotted as a function of time (Fig. 3B and C). To assess the reaction
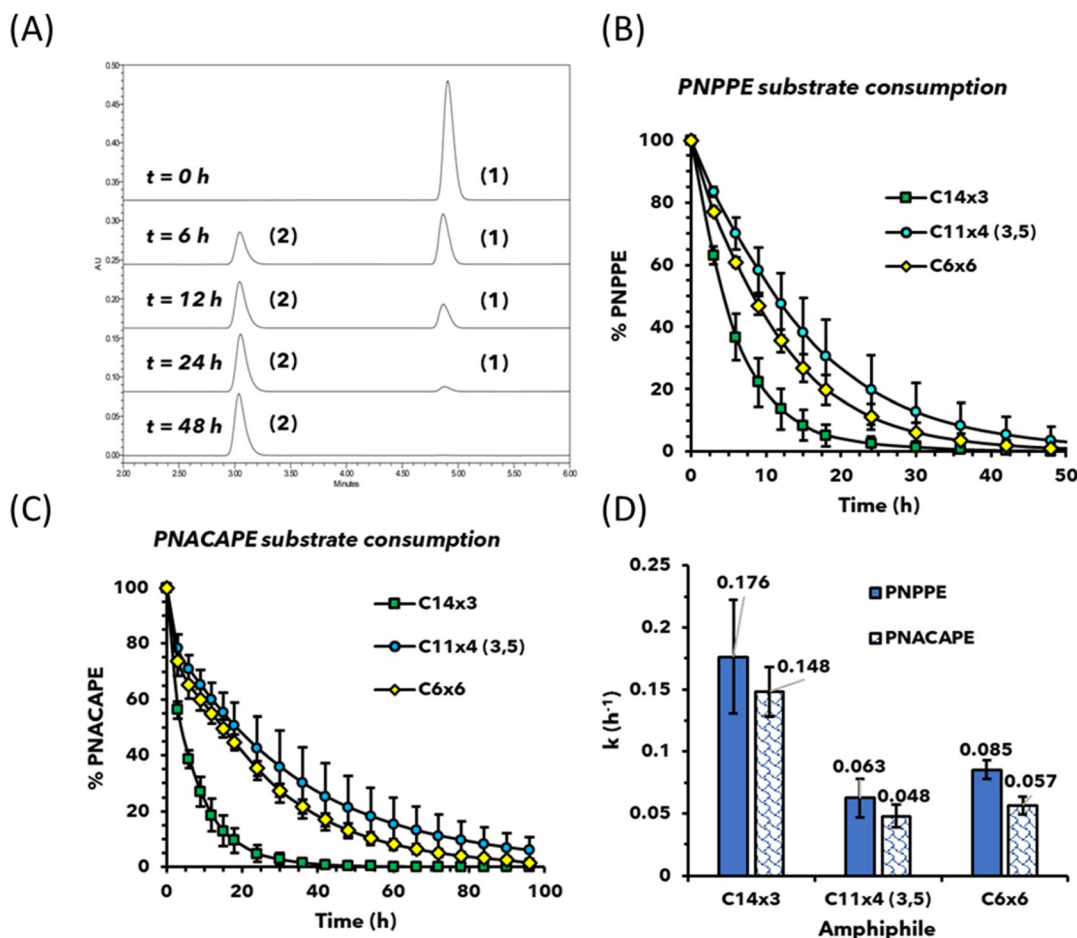
Fig. 3 (A) Representative HPLC chromatogram overlay (taken at 307 nm), showing the transformation of **PNPPE** (**1**) to *para*-nitrophenol (**PNP**) (**2**) using Pd^{II} loaded **C14×3** amphiphilic micelles ([Amphiphile] = 320 μM, [PNPPE] = 300 μM, [Pd(OAc)$_2$] = 150 μM, [Pd(OAc)$_2$: Substrate] = 1 : 2). Normalized substrate consumption of (B) **PNPPE** and (C) **PNACAPE** over time in the presence of **C14×3** (square, green), **C11×4 (3,5)** (circle, deep sky blue) and **C6×6** (diamond, yellow) metallic micelles. (D) Rate constants of **PNPPE** (blue, solid fill) and **PNACAPE** (blue, shingle pattern) depropargyla-tion in presence of **C14×3**, **C11×4 (3,5)** and **C6×6** metal loaded micelles.

kinetics, a natural log of the experimental data was plotted against time which provided a linear equation correlating with a pseudo first-order reaction $\ln[A] = -kt + \ln[A]_0$. The rate constant (k) values were calculated from the slope of the kinetic data, and the theoretical half-life ($t_{1/2}$) values were calculated using the equation $t_{1/2} = \ln(2)/k$. The rate constant k and calculated values of $t_{1/2}$ are presented alongside the experimental value of $t_{1/2}$ in Table S1.†

The kinetic results showed that micelles made with **C14×3** amphiphile were two and a half times faster in performing depropargylation than micelles made from **C6×6** and **C11×4 (3,5)** amphiphiles, while the **C11×4 (3,5)** being the slowest of the three (Fig. 3B and C). The difference in depropargylation rates between **C6×6** and **C11×4 (3,5)** amphiphiles was small compared to **C14×3** (Fig. 3D).

Importantly, the kinetic trends among the three amphiphiles remained the same for both **PNPPE** and **PNACAPE** substrates, although the depropargylation of the latter was slower for all three micellar nanoreactors.

ICP-MS measurements were conducted to ensure that all the micellar nanoreactors had similar Pd^{II} concentrations for a particular substrate and that the obtained trends resulted solely from the architectural changes in the amphiphiles (Fig. S45 and S46†).

2.2. The effect of the length of the end-group on the kinetics of depropargylation

Next, we aimed to investigate if the number of carbon atoms in the end-groups affected the kinetic results. Towards this, mPEG$_{5k}$-D-(C7)$_6$, *i.e.*, **C7×6**, was synthesized and compared with **C14×3** to assess their ability to conduct the depropargylation reactions, since both **C7×6** and **C14×3** amphiphiles have a total of forty-two carbon atoms in their end-groups. The **C7×6** amphiphile was synthesized using the same method employed for the **C6×6** amphiphile by preparing the dendron followed by coupling it to mPEG$_{5k}$-NH$_2$ (Fig. S10†). As seen in Tables 1 and 2, **C7×6** and **C14×3** based micelles had nearly identical CMCs and diameters (4 μM and ~20 nm respectively).

Table 2 Molecular properties of the **C7×6**, **C11×3**, and **C11×4 (3,4)** amphiphiles and their micellar assemblies

Hybrid	Name	End-group	$M_n{}^a$ (kDa)	$M_n{}^b$ (kDa)	$Đ^b$	CMC^c (µM)	$D_h{}^d$ (nm) [Pd] = 0 µM	$D_h{}^e$ (nm) [Pd] = 75 µM	$D_h{}^f$ (nm) [Pd] = 150 µM
mPEG$_{5k}$-D-(C7)$_6$	**C7×6**	n-C$_7$H$_{15}$	6.2	5.7	1.07	4 ± 1	21 ± 2	20 ± 1	19 ± 3
mPEG$_{5k}$-D-(C11)$_3$	**C11×3**	n-C$_{11}$H$_{23}$	6.0	5.7	1.04	5 ± 1	15 ± 1	15 ± 1	15 ± 1
mPEG$_{5k}$-D-(C11)$_4$ (3,4)	**C11×4 (3,4)**	n-C$_{11}$H$_{23}$	6.1	6.6	1.12	6 ± 1	20 ± 1	20 ± 1	18 ± 2

[a] Molecular weight calculated based on a 5 kDa mPEG and the expected exact mass of the dendrons. [b] Molecular weight measured by GPC using PEG commercial standards. [c] Determined using the Nile red method. [d] Hydrodynamic diameter measured by DLS (% volume) of micelles formed from micelles only ([amphiphile] = 320 µM). [e] Hydrodynamic diameter measured by DLS (% volume) of micelles ([amphiphile] = 320 µM) with the encapsulated Pd(OAc)$_2$ salt [75 µM]. [f] Hydrodynamic diameter measured by DLS (% volume) of micelles ([amphiphile] = 320 µM) with the encapsulated Pd(OAc)$_2$ salt [150 µM].

Despite having the same number of carbon atoms in the end-groups, **C14×3** based micelles were almost twice as fast as compared to **C7×6** based micelles at depropargylating both the substrates (Fig. 4). Additionally, the **C7×6** based micelles were approximately 10–15% faster than micelles of **C6×6**. This result is in good correlation with our previous work, which showed that increase in the length of the end-group for a particular architecture leads to faster depropargylation.[26] This highlighted that the architecture had greater influence on the kinetics than the length of the end-groups and the hydrophobicity of the dendron.

Following this comparison, we synthesized an additional amphiphile, mPEG$_{5k}$-D-(C11)$_3$ (**C11×3**), and conducted depropargylation experiments using its micelles, which were then compared with the **C11×4 (3,5)** based micelles. The **C11×3** amphiphile was synthesized using the same method employed for making the **C14×3** amphiphile, using a thiol–ene coupling reaction of mPEG$_{5k}$-triene with 1-undecanethiol to obtain the final amphiphile (Fig. S1†). As seen Fig. 4, it was observed that **C11×3** based micelles were twice as fast as **C11×4 (3,5)** in depropargylating both the substrates. The overall rates obtained for **C11×3** were closer to **C14×3** than to **C11×4 (3,5)**, reinforcing the hypothesis that the architecture had a greater influence on the observed kinetics than the length of the end-groups. In this case as well, the depropargylation rates of **C11×3** based micelles were approximately 25% slower than those obtained for **C14×3** based micelles, which aligns well

with our current and previous findings on the contribution of end-group hydrophobicity for the same polymeric architecture.[26]

2.3. Changing the position of the end-groups

To understand the influence of the position of the branches of the dendron on the kinetics, a different isomer of the four-armed amphiphile was synthesized with the 1,2 dimercaptoether containing end-groups in the third and the fourth position, yielding the mPEG$_{5k}$-D-(C11)$_4$ (3,4) amphiphile, i.e., **C11×4 (3,4)**. The synthetic procedure was similar to the **C6×6** amphiphile where the **C11×4 (3,4)** dendron was first synthesized and then subsequently coupled to mPEG$_{5k}$-NH$_2$ to obtain the final **C11×4 (3,4)** amphiphile (Fig. S6†). As observed in Fig. 5, the **C11×4 (3,4)** based micelles exhibited the fastest kinetics among all the polymers studied. This result was unexpected as the **C6×6** amphiphile, has two of its three 1,2 dimercaptoether moieties located at the third and the fourth position of the aromatic branching unit, similar in their substitution pattern to the two 1,2 dimercaptoether groups of the **C11×4 (3,4)**.

2.4. Anisotropy measurements

To understand the reason for the observed trends in kinetic rates, we aimed to investigate whether the difference in mobility of guest molecules inside the micelles can be correlated
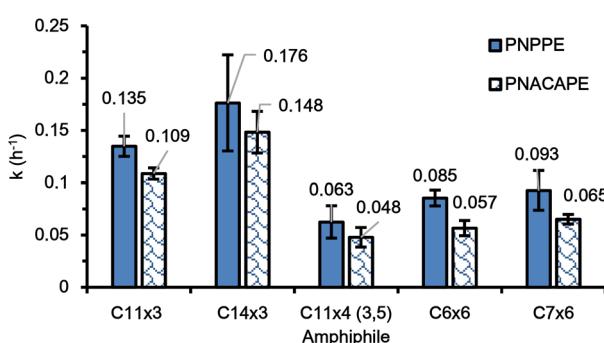
Fig. 4 Rate constants of **PNPPE** (blue, solid fill) and **PNACAPE** (blue, shingle pattern) depropargylation in presence of **C11×3**, **C14×3**, **C11×4 (3,5)**, **C6×6** and **C7×6** metallic micelles.
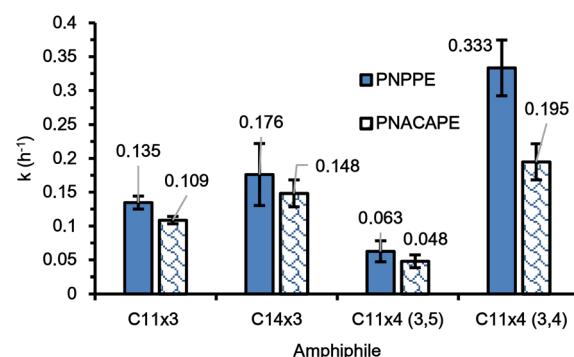

Fig. 5 Rate constants of **PNPPE** (blue, solid fill) and **PNACAPE** (blue, shingle pattern) depropargylation in presence of **C11×3**, **C14×3**, **C11×4 (3,5)** and **C11×4 (3,4)** metallic micelles.

with the difference in depropargylation rates for amphiphiles with different architectures. The mobility of a fluorescent molecule inside the micelles could provide a proxy for the freedom of movement of a substrate molecule inside the core thus ultimately affecting the rates of depropargylation. To calculate the anisotropy factors, we encapsulated Nile Red dye ([Dye] = 21 nM, [amphiphile] = 320 μM), along with various concentrations of Pd(OAc)$_2$ ([Pd] = 0, 75, 150 μM). The

measurements were conducted by placing light polarizers at the source and the detector in different combinations of vertical and horizontal orientations (section 4.3 in ESI†).[40]

The results showed an increase in the anisotropy factor with increasing concentration of Pd(OAc)$_2$ but the value remained the same for all micelles at a given concentration of Pd(OAc)$_2$ with a slight variation of around 5% (Fig. 6). Thus, it was concluded that the Nile Red had approximately the same mobility in the core of the micelles irrespective of their amphiphile's architecture, suggesting that mobility inside the core is not the influence behind the observed trends in the depropargylation kinetics.

2.5. DFT computed binding modes of thioethers/Pd^{II} complexes in different dendrons

To better understand the observed kinetic trends, DFT calculations were carried out using the BP86-D3 method,[41,42] with Ahlrichs' def2-SVP basis set,[43] and with the relativistic effect of palladium that was accounted for by the Stuttgart–Dresden (SDD) effective core potential (ECP).[44,45] Before DFT measurements, we simplified our ligand/Pd^{II} structures based on the results from our previous NMR titration experiments with PEG-dendron amphiphile (3,5-based architecture) and Pd(OAC)$_2$, which showed that only protons adjacent to the sulphur, oxygen, and the aromatic ring, got affected when coordinating with the Pd^{II} salt.[26] Therefore, for these model systems, the structure of the amphiphile was simplified by replacing the PEG chain and dendritic aliphatic end-groups with methyl groups, while preserving the exact architecture of
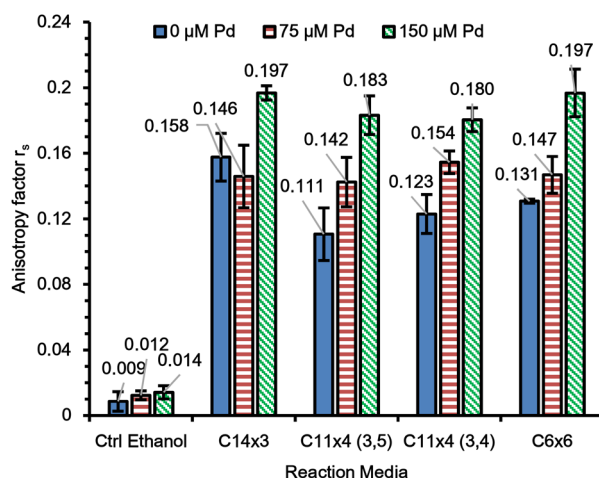

Fig. 6 Anisotropy factor of Nile red dye in amphiphilic micellar environment ([Amphiphile] = 320 μM) at different concentrations of encapsulated palladium acetate. [Pd^{II}] = 0 μM (blue, solid fill), 75 μM (orange, horizontal stripes), 150 μM (green, downward stripes).
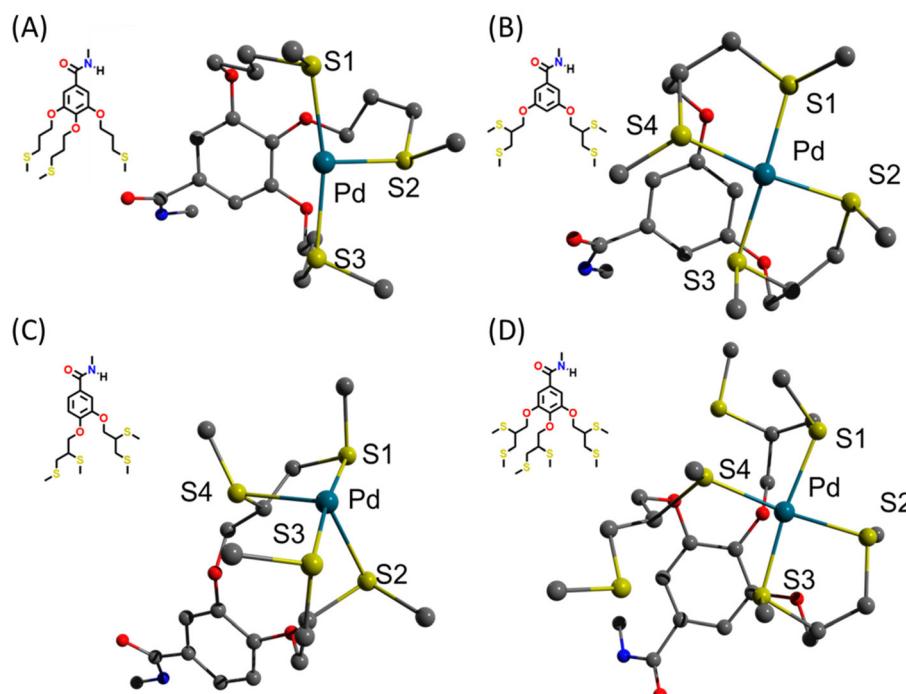

Fig. 7 Simulated results of the predicted orientation of thioethers around the palladium atom (green) in the dendritic structures of (A) three-armed architecture, (B) four-armed (3,5) architecture, (C) four-armed (3,4) architecture and (D) six-armed architecture.

the dendritic cores (Fig. 7). Subsequently, we optimized the geometries of the four model systems and the resulting geometry around Pd^{II} was analysed for each system.

The optimized structure of the Pd^{II}-complex with the three-armed dendron (Fig. 7A) exhibits a T-shaped geometry of the Pd^{II}-center with vacant fourth position that could potentially serve to bind the substrate to the palladium center. The optimized structure of the Pd^{II}-complex with the four-armed (3,4) dendron has a seesaw geometry around Pd^{II}-center, which is atypical and unfavoured in the case of Pd^{II} ion (Fig. 7C). The optimized structures of the Pd^{II}-complex with the four-armed (3,5) and six-armed dendrons both have a square planar geometry, which typical for Pd^{II}-complexes (Fig. 7B and D).[46,47]

The calculated results (Fig. 7) provided important insights into the different reactivities that were observed in the kinetic experiments (Fig. 4 and Fig. 5). While nanoreactors made from four-armed (3,5) and the six-armed dendritic amphiphiles were slowest among the four studied systems, both architectures were shown to have square planar geometry architectures around the Pd^{II}-center, which is a more stable geometry for the Pd^{II}-complex.

On the other hand, the dendritic cores of the other two amphiphiles, which were significantly more reactive, showed atypical seesaw geometry (for the four-armed (3,4) architecture) and a T-shaped geometry (for the three-arm architecture). These unique geometries can be expected to be less stable and hence allows for a better substrate binding, which enables increased reactivity. Overall, the calculated geometries could provide an explanation for the different reactivates observed for the four systems, indicating that the more stable the chelating of the Pd^{II} ions, the less reactive the nanoreactors become. Nevertheless, it is important to note that despite the different geometries, all amphiphiles were shown to maintain the same amount of Pd^{II} ions, demonstrating the critical role of the dendritic core's architecture on the reactivity of the micellar nanoreactors.

3. Conclusions

This work was aimed at understanding the influence of the hydrophobic dendritic core's architecture on Pd^{II}-mediated depropargylation reaction in micellar nanoreactors. Our micellar nanoreactors were based on self-assembled PEG-dendron amphiphiles with palladium acetate as the catalytic species. The ability to synthesize the dendritic block with a high precision enabled us to construct PEG dendron amphiphiles with different dendritic architectures while controlling their HLB and overall molecular weight by changing the number, position and length of the end-groups. These nanoreactors were used to perform depropargylation reactions in PBS with two different propargyl caged substrates, which could potentially be replaced by a propargyl caged prodrug in the future.

The obtained results highlighted how changing the dendritic architecture of the amphiphiles has a greater influence on the depropargylation kinetics than the number and length of the end-groups. In our observations, the micelles based on **C11×4 (3,4)** exhibited the fastest kinetics, surpassing the speed of **C11×4 (3,5)**-based micelles by four to five times. Remarkably, this significantly greater efficiency was observed despite both amphiphiles being isomers with identical atomic composition. The reason for such a drastic difference in the reactivity of micelles with different architectures was elucidated with the help of DFT calculations of the dendritic core of the amphiphile around the Pd^{II} ion. These calculations suggested that **CX×4 (3,4)** architecture should have a highly unlikely seesaw geometry, while the three-armed architecture showed less stable T-shape geometry for their Pd^{II} complexes. These unusual geometries, in contrast to the square planar geometry obtained for the **CX×4 (3,5)** and six-arm amphiphiles, are predicted to be more labile. As a result, they allow Pd^{II} to participate more actively in the depropargylation process compared to the other architectures.

This study highlights how subtle changes in the polymeric architecture can potentially lead to enormous changes in the reaction kinetics for conducting abiotic reactions in aqueous media. Furthermore, when designing micellar nanoreactors for biorthogonally activating prodrugs, we believe these results can serve as a valuable tool for controlling the prodrug activation rate, allowing it to be customized according to the medical requirements of patients.

Author contributions

SW and RJA conceived and designed the project. SW and PR synthesized the amphiphiles and performed the depropargylation experiments. KV helped with performing depropargylation experiments. ST synthesized the PNPPE substrate. RD performed the DFT calculations. AG performed the ICP-MS characterizations. All authors contributed to the interpretation of results and experimental design. SW wrote the manuscript, and all authors revised the final version.

Conflicts of interest

There are no conflicts to declare.

Acknowledgements

References

1 M. Cortes-Clerget, J. Yu, J. R. A. Kincaid, P. Walde, F. Gallou and B. H. Lipshutz, Water as the reaction medium in organic chemistry: from our worst enemy to our best friend, *Chem. Sci.*, 2021, **12**, 4237–4266.

2 B. S. Takale, R. R. Thakore, G. Casotti, X. Li, F. Gallou and B. H. Lipshutz, Mild and Robust Stille Reactions in Water using Parts Per Million Levels of a Triphenylphosphine-Based Palladacycle, *Angew. Chem., Int. Ed.*, 2021, **60**, 4158–4163.

3 J. Epstein, J. J. Kaminski, N. Bodor, R. Enever, J. Sowa and T. Higuchi, Micellar acceleration of organophosphate hydrolysis by hydroximinomethylpyridinium type surfactants, *J. Org. Chem.*, 1978, **43**, 2816–2821.

4 F. Gallou, N. A. Isley, A. Ganic, U. Onken and M. Parmentier, Surfactant technology applied toward an active pharmaceutical ingredient: more than a simple green chemistry advance, *Green Chem.*, 2016, **18**, 14–19.

5 B. H. Lipshutz, The Nano-to-Nano Effect Applied to Organic Synthesis in Water, *Johnson Matthey Technol. Rev.*, 2017, **61**, 196–202.

6 Y. Liu, P. Turunen, B. F. M. De Waal, K. G. Blank, A. E. Rowan, A. R. A. Palmans and E. W. Meijer, Catalytic single-chain polymeric nanoparticles at work: From ensemble towards single-particle kinetics, *Mol. Syst. Des. Eng.*, 2018, **3**, 609–618.

7 M. Artar, E. R. J. Souren, T. Terashima, E. W. Meijer and A. R. A. Palmans, Single Chain Polymeric Nanoparticles as Selective Hydrophobic Reaction Spaces in Water, *ACS Macro Lett.*, 2015, **4**, 1099–1103.

8 Y. Liu, S. Pujals, P. J. M. Stals, T. Paulöhrl, S. I. Presolski, E. W. Meijer, L. Albertazzi and A. R. A. Palmans, Catalytically Active Single-Chain Polymeric Nanoparticles: Exploring Their Functions in Complex Biological Media, *J. Am. Chem. Soc.*, 2018, **140**, 3423–3433.

9 B. H. Lipshutz, S. Ghorai, A. R. Abela, R. Moser, T. Nishikata, C. Duplais, A. Krasovskiy, R. D. Gaston and R. C. Gadwood, TPGS-750-M: A second-generation amphiphile for metal-catalyzed cross-couplings in water at room temperature, *J. Org. Chem.*, 2011, **76**, 4379–4391.

10 B. H. Lipshutz, G. T. Aguinaldo, S. Ghorai and K. Voigtritter, Olefin Cross-Metathesis Reactions at Room Temperature Using the Nonionic Amphiphile "PTS": Just Add Water, *Org. Lett.*, 2008, **10**, 1325–1328.

11 M. Cortes-Clerget, N. Akporji, J. Zhou, F. Gao, P. Guo, M. Parmentier, F. Gallou, J. Y. Berthon and B. H. Lipshutz, Bridging the gap between transition metal- and bio-catalysis via aqueous micellar catalysis, *Nat. Commun.*, 2019, **10**, 1–10.

12 P. Qu, M. Kuepfert, E. Ahmed, F. Liu and M. Weck, Cross-Linked Polymeric Micelles as Catalytic Nanoreactors, *Eur. J. Inorg. Chem.*, 2021, **2021**, 1420–1427.

13 J. Lu, J. Dimroth and M. Weck, Compartmentalization of Incompatible Catalytic Transformations for Tandem Catalysis, *J. Am. Chem. Soc.*, 2015, **137**, 12984–12989.

14 M. Kuepfert, E. Ahmed and M. Weck, Self-Assembled Thermoresponsive Molecular Brushes as Nanoreactors for Asymmetric Aldol Addition in Water, *Macromolecules*, 2021, **54**, 3845–3853.

15 P. Cotanda, A. Lu, J. P. Patterson, N. Petzetakis and R. K. O'Reilly, Functionalized Organocatalytic Nanoreactors: Hydrophobic Pockets for Acylation Reactions in Water, *Macromolecules*, 2012, **45**, 2377–2384.

16 A. Lu, T. P. Smart, I. Thomas, H. Epps, D. A. Longbottom and R. K. O'Reilly, l-Proline Functionalized Polymers Prepared by RAFT Polymerization and Their Assemblies as Supported Organocatalysts, *Macromolecules*, 2011, **44**, 7233–7241.

17 E. Lestini, L. D. Blackman, C. M. Zammit, T. Chen, R. J. Williams, M. Inam, B. Couturaud and R. K. O'Reilly, Palladium-polymer nanoreactors for the aqueous asymmetric synthesis of therapeutic flavonoids, *Polym. Chem.*, 2018, **9**, 820–823.

18 P. Cotanda, N. Petzetakis and R. K. O'Reilly, Catalytic polymeric nanoreactors: More than a solid supported catalyst, *MRS Commun.*, 2012, **2**, 119–126.

19 J. Chen, J. Wang, K. Li, Y. Wang, M. Gruebele, A. L. Ferguson and S. C. Zimmerman, Polymeric 'clickase' Accelerates the Copper Click Reaction of Small Molecules, Proteins, and Cells, *J. Am. Chem. Soc.*, 2019, **141**, 9693–9700.

20 J. Chen, J. Wang, Y. Bai, K. Li, E. S. Garcia, A. L. Ferguson and S. C. Zimmerman, Enzyme-like Click Catalysis by a Copper-Containing Single-Chain Nanoparticle, *J. Am. Chem. Soc.*, 2018, **140**, 13695–13702.

21 Y. Bai, J. Chen and S. C. Zimmerman, Designed transition metal catalysts for intracellular organic synthesis, *Chem. Soc. Rev.*, 2018, **47**, 1811–1821.

22 T. N. Ansari, A. Taussat, A. H. Clark, M. Nachtegaal, S. Plummer, F. Gallou and S. Handa, Insights on Bimetallic Micellar Nanocatalysis for Buchwald–Hartwig Aminations, *ACS Catal.*, 2019, **9**, 10389–10397.

23 M. Bihani, T. N. Ansari, L. Finck, P. P. Bora, J. B. Jasinski, B. Pavuluri, D. K. Leahy and S. Handa, Scalable α-Arylation of Nitriles in Aqueous Micelles using Ultrasmall Pd Nanoparticles: Surprising Formation of Carbanions in Water, *ACS Catal.*, 2020, **10**, 6816–6821.

24 C. Vidal, M. Tomás-Gamasa, P. Destito, F. López and J. L. Mascareñas, Concurrent and orthogonal gold(ɪ) and ruthenium(ɪɪ) catalysis inside living cells, *Nat. Commun.*, 2018, **9**, 1913.

25 P. Destito, A. Sousa-Castillo, J. R. Couceiro, F. López, M. A. Correa-Duarte and J. L. Mascareñas, Hollow nanoreactors for Pd-catalyzed Suzuki-Miyaura coupling and O-propargyl cleavage reactions in bio-relevant aqueous media, *Chem. Sci.*, 2019, **10**, 2598–2603.

26 S. Tevet, S. S. Wagle, G. Slor and R. J. Amir, Tuning the Reactivity of Micellar Nanoreactors by Precise Adjustments of the Amphiphile and Substrate Hydrophobicity, *Macromolecules*, 2021, **54**, 11419–11426.

27 A. Sathyan, S. Croke, A. M. Pérez-López, B. F. M. de Waal, A. Unciti-Broceta and A. R. A. Palmans, Developing Pd(ɪɪ)

based amphiphilic polymeric nanoparticles for pro-drug activation in complex media, *Mol. Syst. Des. Eng.*, 2022, **7**, 1736–1748.

28 M. Pal, K. Parasuraman and K. R. Yeleswarapu, Palladium-catalyzed cleavage of O/N-propargyl protecting groups in aqueous media under a copper-free condition, *Org. Lett.*, 2003, **5**, 349–352.

29 D. Rambabu, S. Bhavani, N. K. Swamy, M. V. Basaveswara Rao and M. Pal, Pd/C-mediated depropargylation of propargyl ethers/amines in water, *Tetrahedron Lett.*, 2013, **54**, 1169–1173.

30 S. E. Coelho, F. S. S. Schneider, D. C. De Oliveira, G. L. Tripodi, M. N. Eberlin, G. F. Caramori, B. De Souza and J. B. Domingos, Mechanism of Palladium(II)-Mediated Uncaging Reactions of Propargylic Substrates, *ACS Catal.*, 2019, **9**, 3792–3799.

31 R. Huang, C. H. Li, R. Cao-Milán, L. D. He, J. M. Makabenta, X. Zhang, E. Yu and V. M. Rotello, Polymer-Based Bioorthogonal Nanocatalysts for the Treatment of Bacterial Biofilms, *J. Am. Chem. Soc.*, 2020, **142**, 10723–10729.

32 J. T. Weiss, J. C. Dawson, K. G. Macleod, W. Rybski, C. Fraser, C. Torres-Sánchez, E. E. Patton, M. Bradley, N. O. Carragher and A. Unciti-Broceta, Extracellular palladium-catalysed dealkylation of 5-fluoro-1-propargyl-uracil as a bioorthogonally activated prodrug approach, *Nat. Commun.*, 2014, **5**, 3277.

33 R. M. Yusop, A. Unciti-Broceta, E. M. V. Johansson, R. M. Sánchez-Martín and M. Bradley, Palladium-mediated intracellular chemistry, *Nat. Chem.*, 2011, **3**, 239–243.

34 A. Unciti-Broceta, E. M. V. Johansson, R. M. Yusop, R. M. Sánchez-Martín and M. Bradley, Synthesis of polystyrene microspheres and functionalization with pd0 nanoparticles to perform bioorthogonal organometallic chemistry in living cells, *Nat. Protoc.*, 2012, **7**, 1207–1218.

35 T.-C. Chang, K. Vong, T. Yamamoto and K. Tanaka, Prodrug Activation by Gold Artificial Metalloenzyme-Catalyzed Synthesis of Phenanthridinium Derivatives via Hydroamination, *Angew. Chem., Int. Ed.*, 2021, **60**, 12446–12454.

36 E. Latocheski, G. M. Dal Forno, T. M. Ferreira, B. L. Oliveira, G. J. L. Bernardes and J. B. Domingos, Mechanistic insights into transition metal-mediated bioorthogonal uncaging reactions, *Chem. Soc. Rev.*, 2020, **49**, 7710–7729.

37 A. J. Harnoy, M. Buzhor, E. Tirosh, R. Shaharabani, R. Beck and R. J. Amir, Modular Synthetic Approach for Adjusting the Disassembly Rates of Enzyme-Responsive Polymeric Micelles, *Biomacromolecules*, 2017, **18**, 1218–1228.

38 E. R. Gillies, T. B. Jonsson and J. M. J. Fréchet, Stimuli-Responsive Supramolecular Assemblies of Linear-dendritic Copolymers, *J. Am. Chem. Soc.*, 2004, **126**, 11936–11943.

39 R. Ramesh, Y. Chandrasekaran, R. Megha and S. Chandrasekaran, Base catalyzed cyclization of N-aryl and N-alkyl-O-propargyl carbamates to 4-alkylidene-2-oxazolidinones, *Tetrahedron*, 2007, **63**, 9153–9162.

40 J. Feng, C. Lin, H. Wang and S. Liu, Gemini dodecyl O-glucoside-based vesicles as nanocarriers for catechin laurate, *J. Funct. Foods*, 2017, **32**, 256–265.

41 Q. S. Li, J. Zhang and S. Zhang, A DFT and ab initio direct dynamics study on the hydrogen abstract reaction of H3BNH3→H2+H2BNH2, *Chem. Phys. Lett.*, 2005, **404**, 100–106.

42 S. Grimme, J. Antony, S. Ehrlich and H. Krieg, A consistent and accurate ab initio parametrization of density functional dispersion correction (DFT-D) for the 94 elements H-Pu, *J. Chem. Phys.*, 2010, **132**, 154104.

43 D. A. Pantazis and F. Neese, All-electron scalar relativistic basis sets for the 6p elements, *Theor. Chem. Acc.*, 2012, **131**, 1292.

44 D. Andrae, U. Häußermann, M. Dolg, H. Stoll and H. Preuß, Energy-adjustedab initio pseudopotentials for the second and third row transition elements, *Theor. Chim. Acta*, 1990, **77**, 123–141.

45 M. Dolg, U. Wedig, H. Stoll and H. Preuss, Energy–adjusted ab initio pseudopotentials for the first row transition elements, *J. Chem. Phys.*, 1987, **86**, 866–872.

46 M. C. MacInnis, R. McDonald and L. Turculet, Synthesis and Characterization of Palladium Complexes Supported by an NPN-Phosphido Ancillary Ligand, *Organometallics*, 2011, **30**, 6408–6415.

47 Q. Yan, L. Zheng, M. Li and Y. Chen, N,S-chelating triazole-thioether ligand for highly efficient palladium-catalyzed Suzuki reaction, *J. Catal.*, 2019, **376**, 101–105.